Molecular Catalysis 545 (2023) 113213

Contents lists available at ScienceDirect

Molecular Catalysis

journal homepage: www.journals.elsevier.com/molecular-catalysis

Investigation of bifunctionality of FePc-functionalized graphene for enhanced ORR/OER activity

Naomi Helsel, Pabitra Choudhury *

Chemical Engineering Department, New Mexico Tech, Socorro, NM 87801 USA

ARTICLE INFO

Keywords:
Catalysis
Electrocatalysis
Overpotential
DFT

ABSTRACT

Iron phthalocyanine monolayer supported on a graphene substrate (GFePc) is a promising Pt-free oxygen reduction reaction catalyst. The electronic properties of GFePc can be tuned via the ligand exchange of FePc, substate doping, and defect incorporation into the graphene substrate. Boron and nitrogen were chosen as substrate dopants due to their comparability to carbon in size. Two of the most common graphene defects, single and double (585) vacancies, were chosen to represent defects that can naturally occur on the graphene substrate. Tetra-substituted phthalocyanines (carboxy-, nitro-, and amino-) and hexadeca-substituted phthalocyanines (chloro-, fluoro-, and amino-) were tested due to their availability in the current market. Utilizing *ab initio* spin polarized density functional theory (DFT) calculations, the dominating pathways of both the oxygen reduction (ORR) and oxygen evolution reactions (OER) have been simulated along with defining their rate-limiting step to quantify the ORR/OER overpotentials (indicator of catalyst reactivity/performance). The DFT results show that ~1 at.% Boron doping in conjunction with a mono-vacancy graphene substrate offers the best ORR performance but a worse OER performance when compared to the pristine GFePc. Generally, an increase in ORR activity exhibited a decrease in OER activity. A qualitative volcano correlation between electronic descriptors and ORR overpotential for modified GFePc systems was observed. The present study allows for expanded understanding and definition of substituted iron phthalocyanine functionalized graphene and the effects of both substrate modification and ligand exchange on GFePc's performance as a potential bifunctional single-metal-atom based electro-catalyst.

Introduction

Designing a bifunctional electrocatalyst capable of performing both oxygen reduction reaction (ORR) and oxygen evolution reaction (OER) efficiently has been a great challenge in the development of alternative energy technology [1,2]. Fuel cells, water splitting, and metal-air batteries are renewable energy sources that either generate chemical fuels or convert chemical energy directly into electricity as an alternative to traditional energy sources such as fossil fuels [3]. Platinum-group metal-based (PGM) catalysts are currently being used to facilitate both ORR and OER. Many PGM-free metal-based catalysts have been investigated to find a catalyst that can balance between ORR/OER activity, electron conductivity, stability, and selectivity. [4]

ORR has sluggish kinetics and finding a replacement ORR catalyst requires the catalyst to have similar or better qualities to the current Pt/C catalyst such as activity, methanol/CO tolerance, and long-term stability [5–8]. Currently, the most efficient OER PGM catalysts are Ir- and Ru-based oxides [9]. No single catalyst has been able to surpass PGM catalysts for both ORR and OER in integrity, stability, and performance [10,11]. The high price of PGM catalysts limits the commercialization of alternative energies with current technology. There has been a lot of research done around finding a replacement catalyst that does not require the use of precious metals. Recent works are showing that single atom catalysts (SACs) such as Ni supported 1 T-$MoSe_2$ [12] or FeN_4/C [13] are nearing/surpassing the commercial Pt/C catalyst ORR overpotential. Additionally, recent works regarding carbon-based catalysts such as LaO_3-graphene [14] and CdN_4C_0-graphene [15] have been investigated to show promising overpotentials. Some of the most researched materials for ORR and OER include metal-nitrogen-carbon complexes, metal-N_4-macrocyclic compounds, and carbon-based materials such as carbon nanotubes and graphene [16–18]. In many cases, it seems that the most promising catalysts that would be able to replace the

Notes: The authors declare no competing financial interest.

* Corresponding author.
E-mail address: pabitra.choudhury@nmt.edu (P. Choudhury).

https://doi.org/10.1016/j.mcat.2023.113213
Received 2 January 2023; Received in revised form 13 April 2023; Accepted 29 April 2023
Available online 3 May 2023

current PGM cathode catalysts include iron as the main metal in these complexes.

Iron phthalocyanine has been studied as a potential cathode catalyst in recent years [19,20]. In those studies, it has been shown experimentally to be an excellent candidate when supported on reduced graphene [20] and theoretically on pristine monolayer graphene [21]. Iron phthalocyanine and graphene materials are readily-available commercially and could serve as a cost-effective catalyst. In our previous study, we introduced elementary ligand exchanges (NH_2- and F-), and substrate doping (N- and B-) and studied the effect on ORR [22]. To build upon our previous work, in the present study we have incorporated vacancies into the graphene substrate and have introduced a larger variety of ligand exchanges in order to study their effects on both ORR and OER.

Computational methods

The Vienna Ab-Initio Simulation Package (VASP) was used to carry our spin-polarized density functional theory calculations (DFT) [23–26]. The interactions between valence electrons and frozen cores were described using the Perdew-Burke-Ernzerhof (PBE) [27,28] form of the generalized gradient approximation (GGA). The projected-augmented wave (PAW) method [29,30] was used with a 400 eV energy cut off. Van der Waal interactions were accounted for using, a semiempirical scheme proposed by Grimme (DFT-D2) in all of our calculations [31]. The Gaussian smearing method with a width of 0.05 eV around the fermi level was used to facilitate convergence. Electronic energies were converged to 10^{-6} eV and ionic relaxations were performed until the residual forces on the atom were less than 0.02 eV/Å.

The single layer, slab model graphene sheet with an optimized C—C bond length (1.42 Å) was used for each system. The FePc-functionalized graphene surface is periodic in the x and y directions with supercell dimensions of 17.07 × 14.78 Å and 21.33 × 22.16 Å. In both cells, the z dimension was chosen to be 25 Å to ensure negligible interactions between periodic images. The smaller cell was used for the substrate modifications and the fluorine ligand substitution. The larger cell was used for the remaining ligand exchanges as the functional groups required more space to ensure negligible interactions between periodic images. A 3 × 3 × 1 Monkhorst-Pack k-point mesh was used to sample the Brillouin zone in all calculations except for the Density of States (DOS) calculations, in which a 9 × 9 × 1 Monkhorst-Pack k-point mesh was used instead.

The determination both the ORR and OER free energy landscapes are discussed in detail in our previous publications [2,21,32]. For ease of calculation, a pH of 0 was used to negate the effects that pH has on the overpotential. These effects are described in the previous publications [32,33]. The free energies of hydrogen molecules were calculated using a combination of both computational and experimental results. The free energies of hydrogen molecules were calculated using a combination of both computational and experimental results. The free energy of O_2 was obtained from the reaction $O_2 + 2H_2 = 2H_2O$; the free-energy change for this equation is 4.92 eV [21,34]. The free energy of H_2O was calculated in the gas phase with a pressure of 0.035 bar that is in equilibrium with liquid water at 300 K [35]. The free energies of surface-bound species were calculated using the TAMkin program [36] by implementing finite temperature thermodynamic model calculations ($G = H - TS$). The remaining calculations are discussed in detail in the supporting information and in our previous publications [21,32]. The values required for the calculation of Gibbs free energy can be found in Table S1. The GFePc and GFePcAQ values can be found in our previous publication. [21]

Results and discussion

As stated previously, the focus of the present study is modified iron phthalocyanine functionalized graphene (GFePc). The pristine GFePc can be found in Fig. 1 and more detail regarding the structure specifications of pristine GFePc can be found in our previous publication [21].

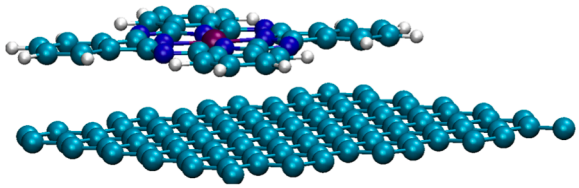

Fig. 1. Schematic representation of iron phthalocyanine functionalized graphene. Blue, purple, cyan, and white represent N, Fe, C, and H, respectively.

As seen in Fig. 1, iron phthalocyanine (FePc) can be supported on the 2D graphene substrate which sets the expectation of the catalyst to behave like a metal oxide.

Without any support, FePc is prone to aggregation which leads to fewer active sites available for catalytic process. Additionally, FePc suffers from poor electron conductivity [20]. Carbon nanotubes [37], Vulcan XC-72 [38], and reduced graphene [20] have been studied in conjunction with FePc to improve its catalytic activity. Jiang et al. published a study regarding a catalyst with chemical reduced graphene supporting iron phthalocyanine that was shown through experiment to have comparable current density to commercial Pt/C. In that publication, Jiang et al. mentions that the FePc is immobilized by π-π interactions onto the graphene sheets. Additionally, as the FePc was homogenously attached, supplementary electron-providing sites were formed [20]. The stability of GFePc, BGFePc, and their intermediates has been investigated computationally as a function of potential and pH in our previous work. Those results suggested that both catalysts would be stable in the regions of potential and pH at the operating conditions required of rotating ring disk experiments and PEM fuel cells [39].

Iron (II) phthalocyanine and ligand substitution

FePc can be seen in a top-down view in Fig. 2. This molecule can be modified by substituting some or all the hydrogens present on the exterior of the carbon rings. Substituting functional groups in for the *hydrogens* affects the overall electronic properties of the molecule through Inductive and Mesomeric effects. These substitutions may also change FePc's ability to conduct charge transfer towards catalytic processes such as ORR/OER. The substitutions were chosen based on what modifications were available to purchase commercially through suppliers such as PorphryChem.

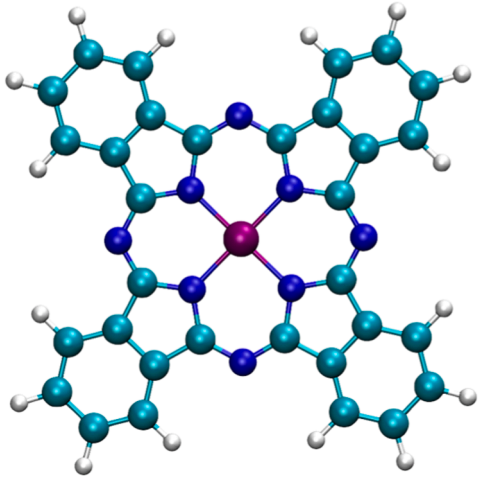

Fig. 2. Schematic representation of iron phthalocyanine[32]. The blue, purple, cyan, and white spheres represent N, Fe, C, and H, respectively.

Inductive and Mesomeric effects

Different ligands substituted onto FePc allow for different properties that can be explained through Inductive and Mesomeric effects. In both effects, the substituent can either be an electron releasing (+) or electron withdrawing (-) group/element.

The Inductive effect, which is based on the polarization of sigma bond by the difference in electronegativities, is negatively (*-I*) present in the following groups presently studied from largest to smallest: NO_2 > COOH > F > Cl > NH_2 > H. This means that the most electron withdrawing group studied is NO_2-.

The Mesomeric effect, which is based on resonance structures of a group caused by the delocalization of electrons is both positively (*+M*) and negatively (*-M*) present in presently studied groups with resonance structures. NO_2 has a *-M* effect and is considered an electron withdrawing group. NH_2 has a *+M* effect, which means that it is considered an electron releasing group based on resonance structures alone. The Mesomeric effect is considered to be stronger than the inductive effect which means that though NH_2 has a *-I* effect, its *+M* effect dominates, and it is considered to be electron releasing.

Types of substitutions

Full substitutions were the cases in which all hydrogens in FePc were replaced with another group and is shown in Fig. 3. Amine (NH_2-), fluorine (F-), and chlorine (Cl-) were the groups considered.

Para- and Meta- substitutions were the cases in which four hydrogens in FePc were replaced from the 16-hydrogen total is shown in Fig. 4. The para- groups considered were nitro (NO_2-), carboxy (COOH-), and amine (NH_2-). Amine (NH_2-) was also considered in the meta- orientation. Having both para- and meta- amine systems allows for insight regarding how orientation effects the catalyst's performance.

Having a variety of groups with differing strengths of electron withdrawing effects and a group with electron releasing effects allows us to get a bigger picture into how substituting these groups effects catalytic charge transfer. As mentioned previously, the preferred ligand orientations were determined through finding out what modifications of FePc were available to purchase through commercial suppliers.

Graphene substrate

The graphene substrates utilized in both the 17.07 × 14.78 Å and 21.33 × 22.16 Å cells are shown in Fig. 5. The systems that could fix into the smaller cell, which included substrate effects and fluorine substitution, had a substrate simulated with 96 carbons. This was done to reduce computational cost and the remainder of the systems, which included most of the ligand substitutions and combination ligand substitution and substate dopant, were simulated in the larger cell with 180 carbons.

Doping & defects

The graphene substrate was modified through substrate doping and vacancy incorporation. Nitrogen and Boron were chosen as the main dopants due to their similarity in size and properties to carbon which results in the least amount of lattice deformation. The dopants were simulated to be directly under the metal center as in our previous publication regarding substrate doping, they were found to be the most favorable site through FePc's binding energy to the graphene [32]. The dopants were simulated to be at ~1 at.% (1:95 ratio). The dopants incorporated into the graphene substrate directly under the FePc metal center is shown in Fig. 6. Single and double (585) vacancies in the graphene substrate were also simulated as these type of defects can be experimentally synthesized [40,41]. The double vacancy preferred to be oriented under the metal center while the single vacancy preferred to be away from the metal center. The vacancies and their locations can be seen in Fig. 7. These were also simulated at ~1 at.% (1:95 ratio).

The effect of increased boron doping percentage was explored. As shown in Fig. 8, ~2 (2:94 ratio) and ~3 at.% (3:93. ratio) boron doping was worked with as to not introduce too much change into the graphene lattice. Boron was used as it was found to be the best guess system for doping alone. Two different orientations were simulated, however, the systems in which at least one boron atom was present underneath the metal center had the highest binding energies. The effect of a combined ~1 at.% Boron doping and vacancy incorporation was tested. Testing combinations with both vacancy types, each system favored the boron directly below the metal center while the vacancies were away from the metal center. These substrates are depicted in Fig. 9. The effect of a combined ~0.55 at.% Boron doping (1:179) and NH_2- ligand substitution was investigated. Since the amine group was simulated in the larger supercell, the doping percentage was ~0.55 at.% rather than ~ 1%. In Fig. 10, the combination system is shown.

Oxygen reduction reaction and oxygen evolution reaction

The Oxygen Reduction (ORR) and evolution (OER) reactions being simulated in the form of free energy landscapes to find computational ORR/OER overpotentials, which is essentially the largest reaction barrier of the given elementary steps. The overpotential of a catalyst serves to be a reliable catalytic activity descriptor for theoretical calculations. ORR, OER, and the importance of overpotentials have been described in detail in previous publications [2,21,32,33]. Previous DFT calculations show that the dominating ORR mechanism is the associative mechanism in which a direct four-electron transfer occurs [21]. The OER equation and subsequent steps are the reverse order of the ORR reaction. The

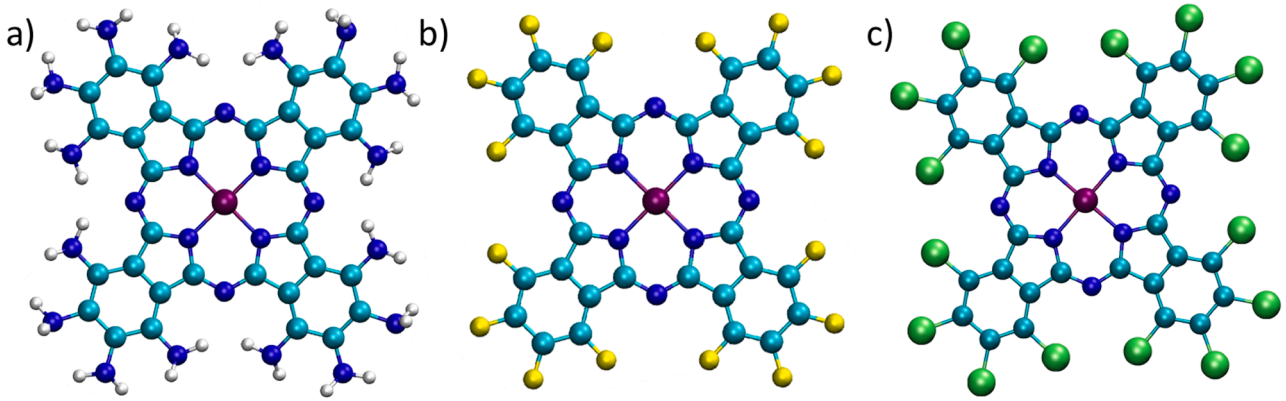

Fig. 3. Schematic representation of iron phthalocyanine with full a) NH_2, b) fluorine, and c) chlorine ligand substitution. Blue, purple, cyan, white, yellow, and green represent N, Fe, C, H, F, and Cl, respectively.

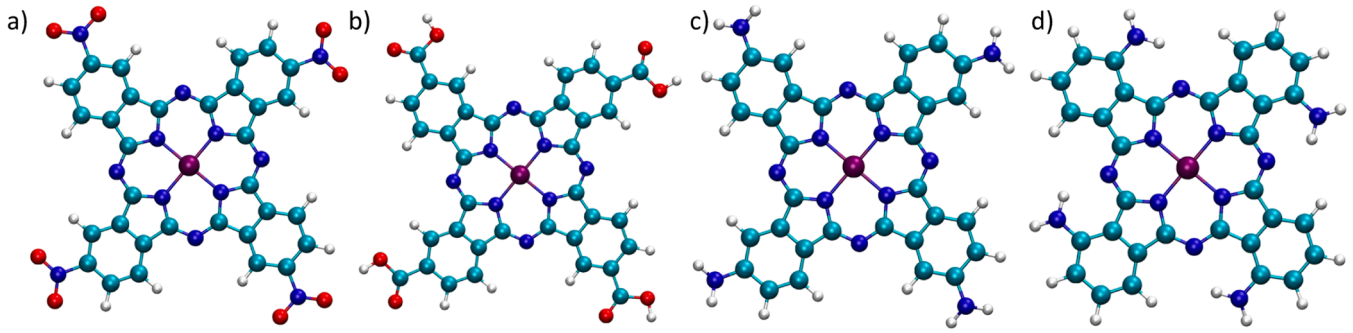

Fig. 4. Schematic representation of iron phthalocyanine with para- a) NO_2, b) COOH, c) NH_2 and meta- d) NH_2 ligand substitution. Blue, purple, cyan, white, and red, represent N, Fe, C, H, and O, respectively.

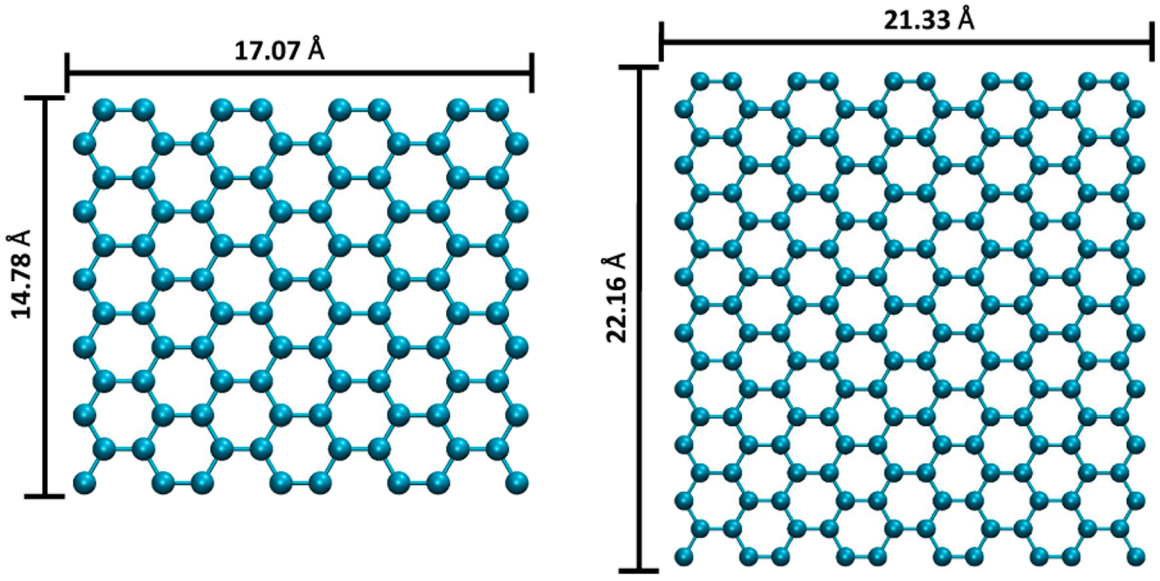

Fig. 5. Schematic representation of a) 96-carbon atom (17.07×14.78 Å) and b) 180 carbon atom (21.33×22.16 Å) graphene substrates. Cyan represents carbon.

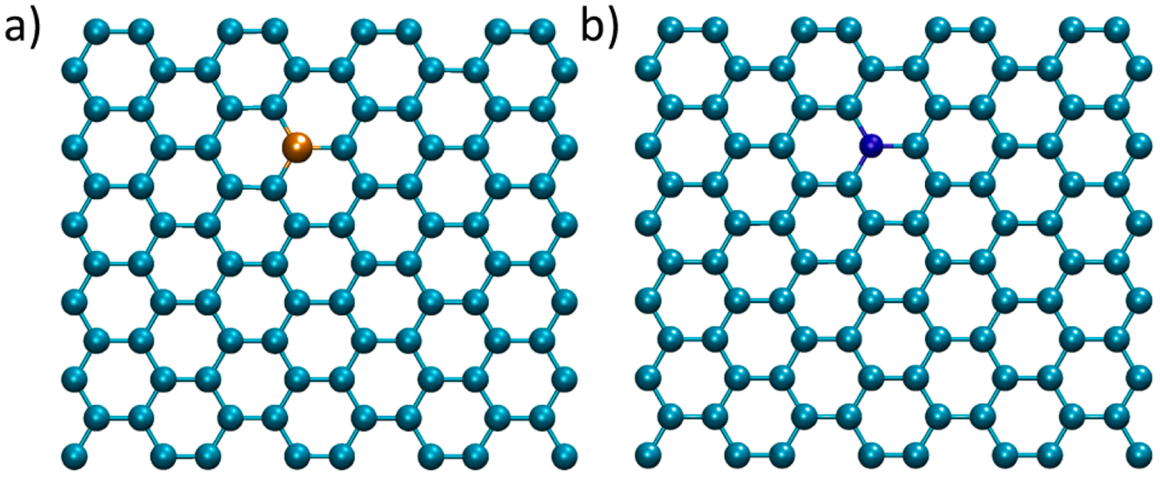

Fig. 6. Schematic representation of the 96-carbon atom graphene substrate (17.07×14.78 Å) cell doped with a) boron and b) nitrogen. Cyan, orange, and blue represent carbon, boron, and nitrogen respectively.

overall ORR reaction equation and its elementary steps are shown in Table 1.

Free energy landscapes, which are visual representations of the elementary reaction steps can be generated of both ORR/OER. However, since ORR and OER are the reverse reactions of one another, only the ORR free energy landscape of MB+SD-GFePc is shown in Fig. 11 as an example. The ΔG of each reaction step for all systems can be found in Table S2 for both ORR and OER. Consistent with our previous

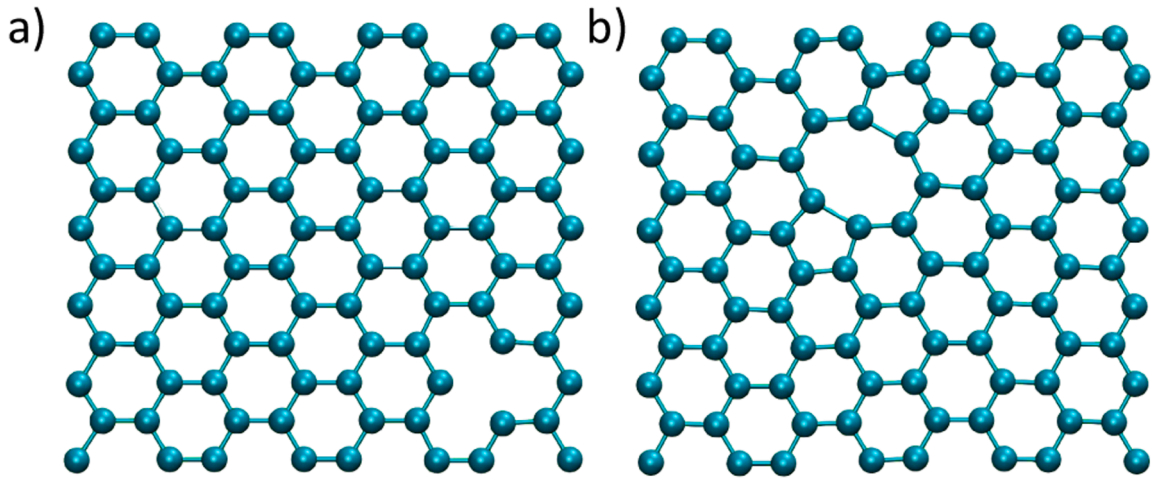

Fig. 7. Schematic representation of the 96-carbon atom graphene substrate (17.07×14.78 Å) cell with a) single and b) double vacancies. Cyan represents carbon.

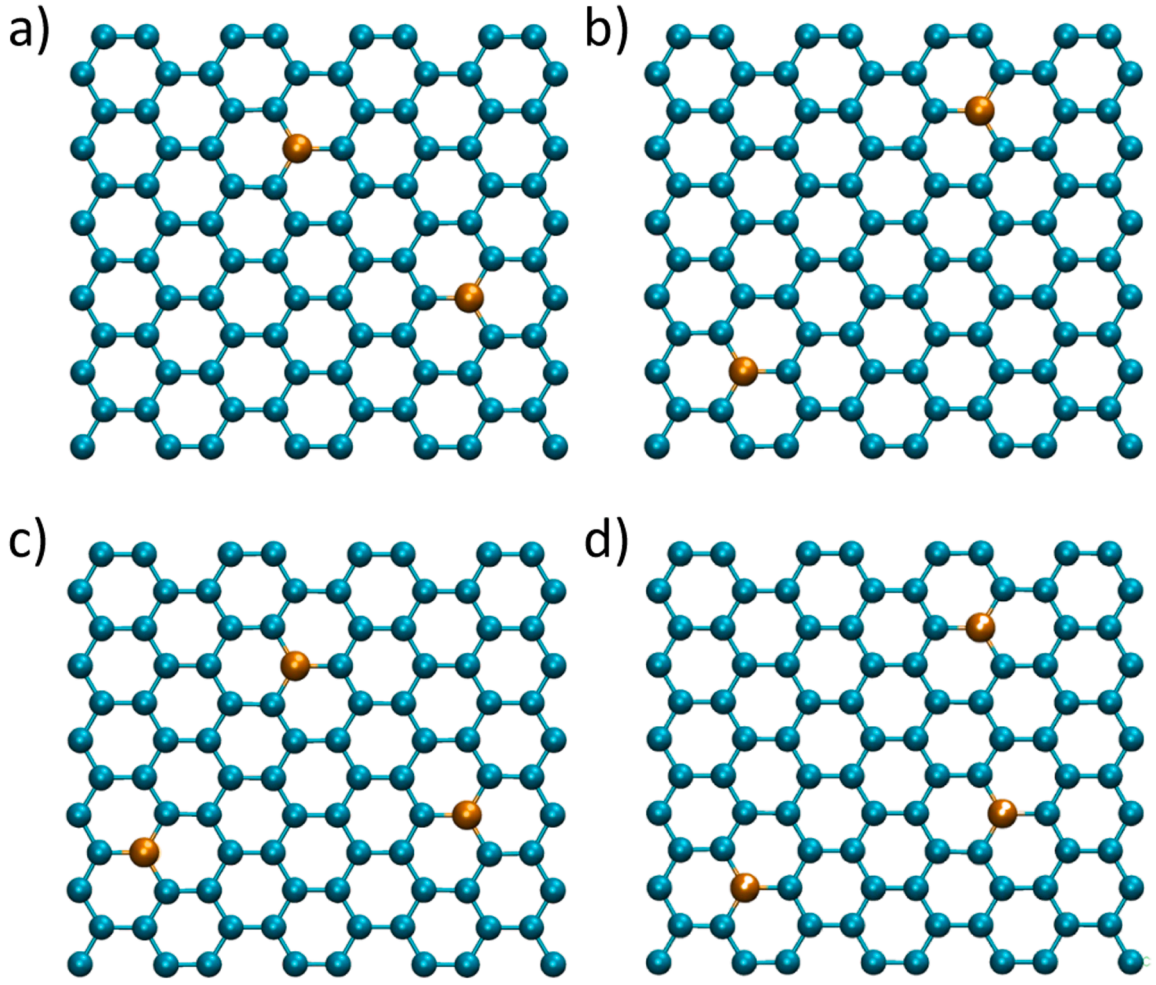

Fig. 8. Schematic representation of the 96-carbon atom graphene substrate (17.07×14.78 Å) cell doped with an increased percentage of boron. At ~2 at.%, the a) favorable / b) unfavorable configuration and ~3 at.%, c) favorable / d) unfavorable. Cyan and orange represent carbon and boron, respectively.

publications [21,32], the ORR rate-limiting step at maximum fuel cell operating conditions (U = 1.23 V) for all tested systems is the first reduction step in which O_2* reacts with a $H^+$and an electron to form HOO* on the surface of the catalyst. The OER rate-limiting step was also found to be the first reduction step in which O* reacts with H_2O to form OOH* at maximum fuel cell operating conditions (U = 1.23 V) for all tested systems.

The ORR/OER overpotentials for all tested systems are displayed in Table 2. When looking at the catalysts tested, typically when the ORR performance is enhanced by a particular system modification, the OER

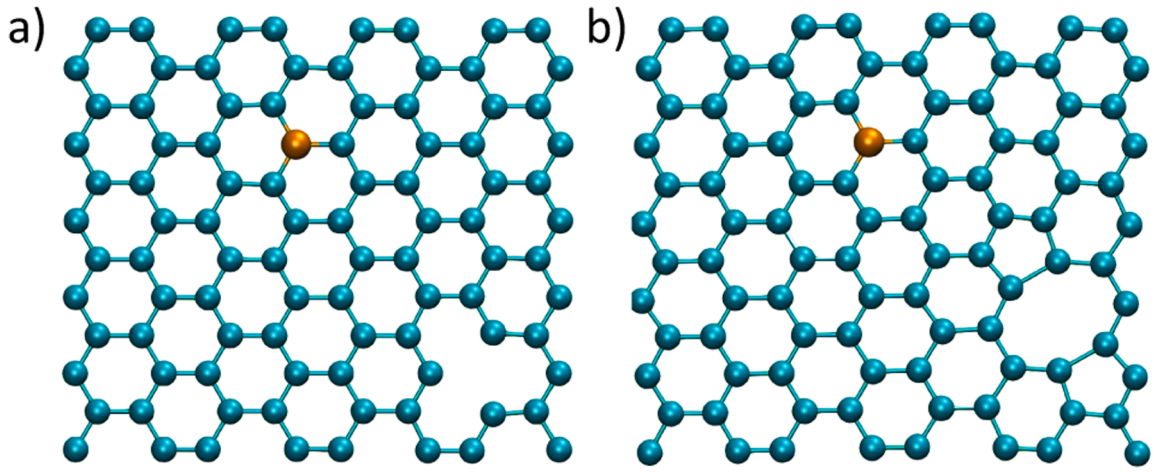

Fig. 9. Schematic representation of the 96-carbon atom graphene substrate (17.07×14.78 Å) cell doped with a combination of boron doping with a) single and b) double (585) vacancy presence. Cyan and orange represent carbon and boron, respectively.

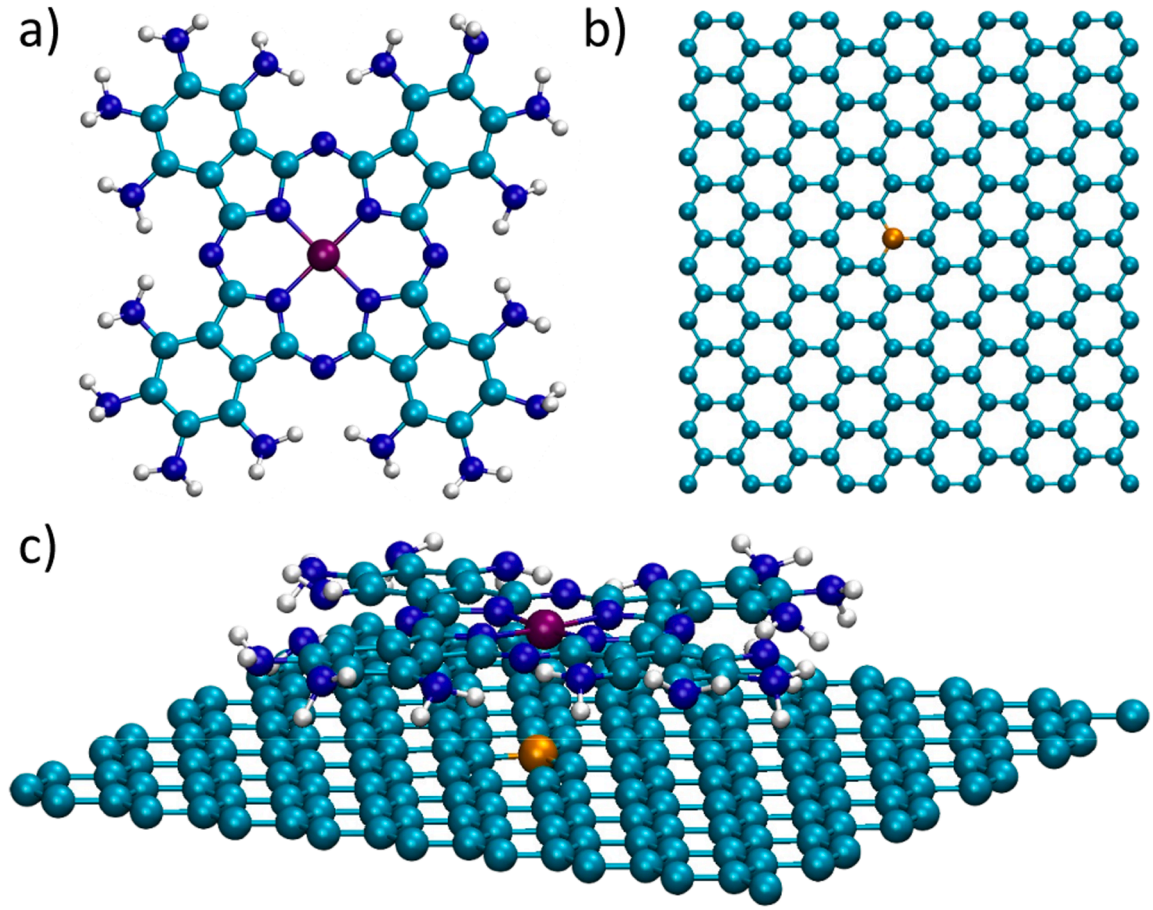

Fig. 10. Schematic representation of a) iron phthalocyanine with a full NH_2 ligand substitution, b) ~0.55 at.% Boron-doped 180 carbon atom (21.33×22.16 Å) graphene substrate, and c) NH_2 substituted iron phthalocyanine functionalized boron-doped graphene. Blue, purple, cyan, white, and orange, represent N, Fe, C, H, and B, respectively.

overpotential sees an increase when compared to the pristine GFePc. The best-guess systems along with nitrogen doping as a comparison were chosen to incorporate solvation corrections which introduces a water-solvated environment, rather than DFT's vacuum environment. A continuum solvation model [42,43] is used and is explained in detail in previous publications. [21,32,44-47]

Substrate doping

When introducing only substrate doping into the GFePc structure, boron-doped graphene (BGFePc) offered the largest reduction in ORR overpotential between boron and nitrogen ~1 at.% dopants. Notably, the ~1 at.% Nitrogen doped graphene system (NGFePc) offered a lower OER overpotential than the BGFePc system but not lower than the

Table 1
Overall reaction and elementary reaction steps of ORR mechanism.

Overall ORR Mechanism
$O_{2\ (g)} + 4(H^+ + e^-) \rightarrow 2H_2O_{(g)}$
Elementary Reaction Steps
$O_{2\ (g)} \rightarrow O_2^*$
$O_2^* + (H^+ + e^-) \rightarrow HOO^*$
$HOO^* + (H^+ + e^-) \rightarrow H_2O_{(g)} + O^*$
$O^* + (H^+ + e^-) \rightarrow + HO^*$
$HO^* + (H^+ + e^-) \rightarrow H_2O_{(g)}$

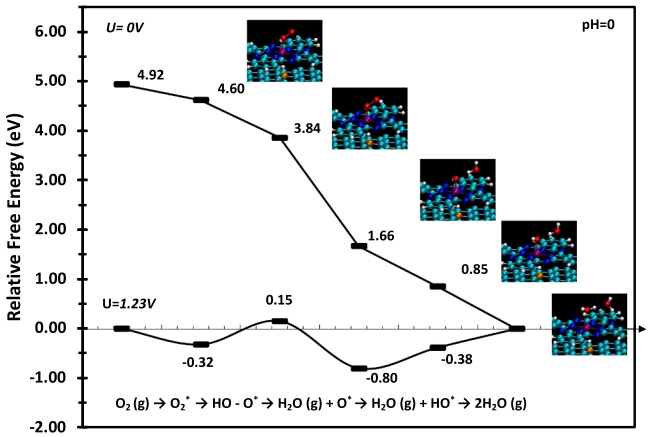

Fig. 11. Associative mechanism electrocatalytic reaction free-energy landscapes of ORR followed by complete WFR steps at two different electrode potentials (0 and 1.23 V) in a vacuum environment for MB+SD-GFePc. The energies are relative to two water molecules produced on the MB+SD-GFePc surface, for which a free-energy change is 4.92 eV.

Table 2
ORR and OER overpotentials for pristine GFePc, all of its modified varieties, and solvation corrections which are denoted with 'AQ' at the end.

		Overpotential (eV)	
Type	System	ORR	OER
Pristine	GFePc	0.76	0.85
Substrate Doping	1-NGFePc	0.8	0.98
	1-BGFePc	0.63	1.06
	2mn-BGFePc	0.61	1.01
	3mn-BGFePc	0.63	1.02
	2n-BGFePc	0.65	1.04
	3n-BGFePc	0.63	1.05
Vacancies	SD-GFePc	0.63	1.05
	585-GFePc	0.67	1.05
Substrate Doping & Vacancies	MB+SD-GFePc	0.59	0.94
	MB+585-GFePc	0.61	0.97
Ligand Substitution	16F-GFePc	0.74	0.99
	16NH_2-GFePc	0.69	1.10
	Para-NH_2-GFePc	0.65	1.07
	Meta-NH_2-GFePc	0.64	1.07
	Para-NO_2-GFePc	0.75	0.88
	Para-COOH-GFePc	0.76	0.99
	16Cl-GFePc	0.76	0.93
Substrate Doping & Ligand Substitution	16NH_2-1B-GFePc	0.67	1.07
Solvation Corrections	GFePcAQ	0.68	0.83
	NGFePcAQ	0.78	0.88
	BGFePcAQ	0.49	1.00
	MB+SD-GFePcAQ	0.47	0.95

pristine GFePc. Solvation corrections were completed for both BGFePc and NGFePc. In the case of BGFePc, the ORR overpotential was lowered to 0.49 eV (~0.14 eV difference) and the OER overpotential was lowered to 1.00 (~0.05 eV difference). In the case of NGFePc, the ORR overpotential was lowered to 0.78 eV (~0.02 eV difference) and the OER overpotential was lowered to 0.88 eV (~0.10 eV difference which is closer to the solvation corrected pristine GFePc OER overpotential (0.83 eV). It is interesting to note that BGFePc, which was more favorable towards ORR, had a larger reduction in ORR overpotential than OER overpotential when solvation corrections were incorporated. This ideology continues with NGFePc, that was more favorable towards OER, and had a larger drop in OER overpotential than ORR overpotential.

Increased boron doping (~2 and ~3 at. doping%) was also explored to view its effect on ORR and OER overpotential. As noted in our previous publication, graphene substrate boron doping between ~1–3 at.% offers no significant change in either ORR or OER overpotentials between the more favorable and less favorable configurations of ~2 and ~3 at.% [32]. However, it is important to note that when increasing the doping percentage of any element into the graphene lattice past a certain point (relative to that element's similarity to carbon) will introduce a great amount graphene lattice deformation and lead to significantly decreased stability. It is acknowledged that increasing the doping percentage past the ~3 at.% tested may negatively affect the overall stability and activity of BGFePc as is true with any doping element.

Vacancies

Both the single and double vacancies systems were found to have a favorable effect on ORR, while hindering OER. However, the single vacancy, when placed away from the metal center, enhanced the ORR overpotential to a similar effect to that of the boron-doped systems mentioned previously while the double (585) vacancy placed under the metal center offered slightly less of a reduction of ORR overpotential. When compared to the pristine GFePc, the OER overpotential increased by 0.20 eV in both vacancy cases. This high OER overpotential, as is true for the substrate dopants, indicates that these substrate effects greatly hinder OER while enhancing ORR, and suggests a potential balance between the two overpotentials that is dependent on the initial pristine GFePc structure.

Substrate doping and vacancies

As noted previously, the single vacancy in the graphene substrate enhanced the ORR overpotential to a similar degree to that of the boron-doped systems. Because of this, both modifications were combined into the same graphene substrate to study their combined effect (MB+SD-GFePc). This combination offered a slight reduction in ORR overpotential and larger reduction in OER overpotential when compared to either substrate modification on its own. As MB+SD-GFePc offered the lowest ORR overpotential and a moderate OER overpotential, solvation corrections were also performed for this system. When incorporating solvation corrections, the ORR overpotential was lowered to 0.47 eV (~0.12 eV difference) and the OER overpotential was lowered to 0.95 (~0.10 eV difference). Though the ORR overpotential saw a slightly larger drop than the OER overpotential, it was more balanced that previously noted for the BGFePc and NGFePc solvation corrections.

The combination of a double vacancy and boron doped substrate was also tested (MB+585-GFePc) even though the double vacancies effect on ORR wasn't as pronounced as the single vacancy case. When combined, the Boron doping, and double vacancy substrate offer similar ORR and OER overpotentials to MB+SD-GFePc with only 0.02 and 0.03 eV differences between the two overpotentials respectively. However, since the MB+585-GFePc ORR and OER overpotentials were slightly higher than MB+SD-GFePc and not a best guess system, solvation corrections were not performed.

Ligand substitution

When studying the ligand substitutions made to FePc, the amino systems (16NH_2-GFePc, Para-NH_2-GFePc and Meta-NH_2-GFePc) offered the most reduction in ORR overpotential, while increasing the OER

overpotential to be between 1.07–1.10 eV. Note that there was no significant difference (only ~0.01 eV difference in ORR overpotential) between the para- and meta- amino configuration which can suggest that the overpotential of GFePc modified systems is independent of ligand location. However, more testing with other ligands is required to draw a definitive conclusion. The amino- ligand group was the only ligand tested that had a positive Mesomeric (+*M*) effect and was considered an electron-releasing group. As the ORR overpotential was ~0.07–0.12 eV lower when compared to the pristine GFePc case, it is suggested that the +*M* effect of the amino- ligand group is favorable to ORR activity.

While the remaining ligand systems (16F-GFePc, 16Cl-GFePc, Para-NO_2-GFePc, and Para-COOH-GFePc) saw little to no reduction ORR in overpotential, they had a lower OER overpotential when compared than the amino systems. These ligand groups each either had a negative Mesomeric (-M) or negative Inductive (-I) effect, which suggests that electron-withdrawing groups are unfavorable to ORR activity and is more favorable to OER than the amino ligand group, but still unfavorable to ORR when compared to the pristine GFePc system. Interestingly, Para-NO_2-GFePc and 16Cl-GFePc offer the closest OER overpotential to pristine GFePc. Para-NO_2-GFePc was the only structure studied that was considered an electron-withdrawing group in both the Inductive and Mesomeric effects (-I and -M). Offering an OER overpotential of 0.88 eV suggests (only ~0.03 eV higher than GFePc's OER overpotential). These findings suggests that the combination of -M and -I effects has no significant negative effect on OER overpotential, but the -I effect alone hinders OER. Future research regarding other ligand substitutions that still offers a -M effect, but weaker -I effect should be explored to see how these effects independently effect OER. Additionally, it is important to note that these two effects can not fully explain the interaction between FePc, the graphene substrate, and the substituted ligands.

Ligand substitution and substrate doping

As both the amino ligand exchange and boron-doping enhanced the ORR overpotential, a combination of 16NH_2-GFePc and BGFePc was explored. It was studied at a slightly lower doping percentage (~0.55 at. %) than BGFePc alone (~1 at.%) due to the size of the supercell used to encompass the ligand substitutions having a larger graphene substrate. The combination of these modifications yielded ORR and OER overpotentials similar to the 16NH_2-GFePc modification alone (~0.02–0.03 eV difference). This suggests that the lower doping percentage had a significantly reduced effect to that of ~1–3 at. boron-doping%. Future research regarding increased boron doping percentage and an ORR activity enhancing ligand substitution, such as the amino- group tested in the present study, should be explored to view the limitations of reducing the ORR overpotential GFePc.

Charge and DOS analyses

To understand the charge transfer of GFePc and each system's respective modification, Bader charge analysis, charge density differences (CDD), and partial density of states (PDOS) were conducted for either the intermediate-free catalyst and/or chemisorbed O_2 intermediate of each studied system depending on the analysis conducted.

Bader charge analyses of both the bare catalyst and chemisorbed O_2 intermediate of each studied system allow for the quantification of initial substrate charge and initial Fe oxidation state, while also accounting for overall oxygen charge accumulation in the chemisorbed O_2 intermediate. The Bader charge analysis values for the aforementioned categories can be found in Table S3. Though only ranging between 1.08 and 1.157, a broad trend was observed when ORR overpotential was plotted against the initial oxidation state of Fe, as shown in Fig. 12. In most cases where the oxidation state was at its highest, the ORR overpotential was at its the lowest.

The trend between the initial Fe oxidation state and the initial

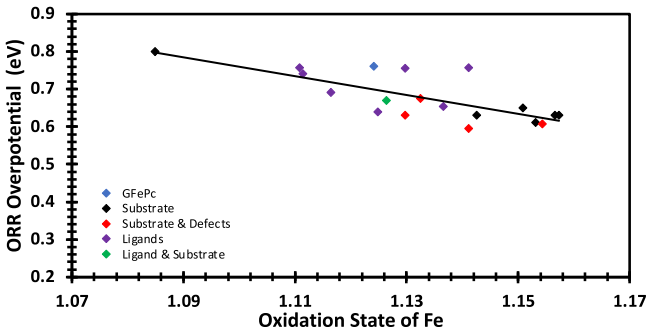

Fig. 12. Oxidation state of Fe explored as a descriptor of overpotential (eV).

substrate charge was explored to determine if there was a correlation between the two descriptors. Though no trend was observed when considering all tested systems, if only the pristine GFePc and any singular or combination of substrate modification were considered a clear trend arose, as shown in Fig. 13a. Note that the far-left black diamond in Fig. 13a is NGFePc, which is the only substrate modification that had an extra electron in the substrate and therefore acted as an N-type dopant. Fig. 13b shows that no trend is present for the same descriptor if only the pristine GFePc and any ligand substitution was considered. This is most likely due to the influence of varying intensities of Inductive and Mesomeric effects on the ligands and FePc molecule that aren't present in the substrate doping modifications.

Shown in Fig. 14, the ORR overpotential was also plotted against the oxygen molecule charge accumulation for the chemisorbed O_2 intermediate. Fig. 14a encompasses all modifications tested and Fig. 14b only incorporates pristine GFePc and the substrate-modified systems. As was true for the previous descriptor comparison, a better trend was observed when excluding the ligand-modified systems when using oxygen molecule charge accumulation as a descriptor of ORR overpotential.

Charge density differences (CDD) and plane-averaged CDD plots of the chemisorbed O_2 intermediate structure of each studied system were analyzed and are shown in Figs. S1-S5. These plots play more a qualitative role in ensuring the proper charge distribution can be seen for each system.

It is known that the number of e_g electrons play a role on ORR activity for at least perovskite oxides to form a volcano trend [48,49]. Because it is difficult to quantify the number of e_g electrons computationally, the bandcenter of the Fe *d* and e_g bands using density of states (DOS) calculations were calculated in lieu of the number of e_g electrons. Furthermore, the DOS of each modified system were calculated to observe how the bandcenters of Fe change with respect to the ligand and/or substrate modification made to GFePc. The bandcenters were calculated using the DOS between −10 and 10 eV, before being adjusted to be relative to the Fermi level. Changing the range at which the bandcenter is calculated drastically changes the location at which the trend in data arises, however, the relative trend remains the same. Fig. 15 shows the *p*-band center and e_g-bandcenter as descriptors of ORR overpotential. With the values at the top of the volcano signifying the more active systems, the systems containing boron doping and/or a single vacancy had the most favorable effects when compared to pristine GFePc. However, this number is relative and represents more of a qualitative aspect of the catalyst. In which, the systems that have the most favorable overpotentials had similar e_g-bandcenters. This suggests that there could be a correlation between e_g-bandcenter and overpotential, which is consistent with our previous publication [32].

Conclusion

The modifications to iron phthalocyanine functionalized monolayer graphene (GFePc) in most of the tested cases offers enhanced ORR activity at the expense of OER activity. Introducing a single vacancy and

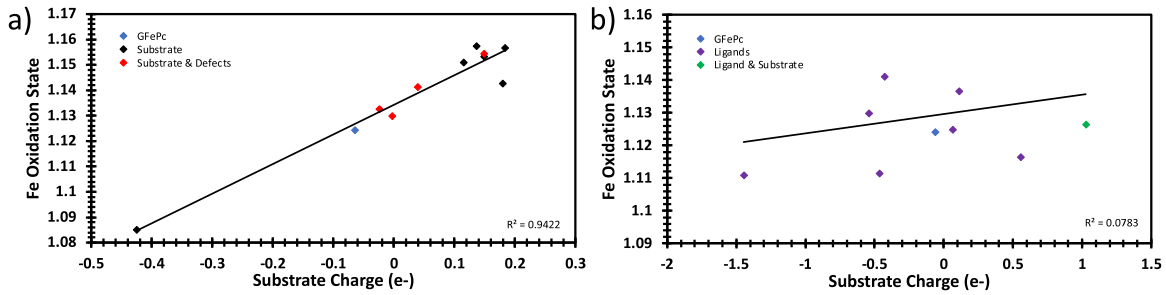

Fig. 13. Oxidation state of Fe plotted against graphene substrate charge (e-) for pristine GFePc and a) substrate-modified systems or b) ligand-modified systems.

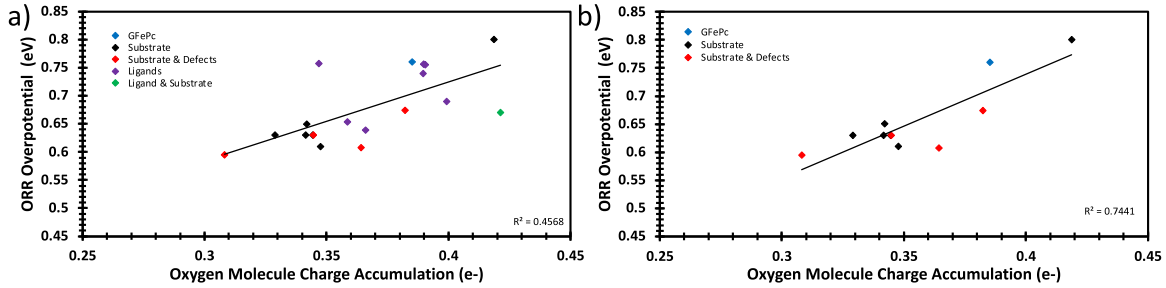

Fig. 14. ORR overpotential plotted against oxygen molecule charge accumulation of the chemisorbed O_2 intermediate for pristine GFePc and a) all tested ligand/substrate modifications or b) only the substrate-modified systems.

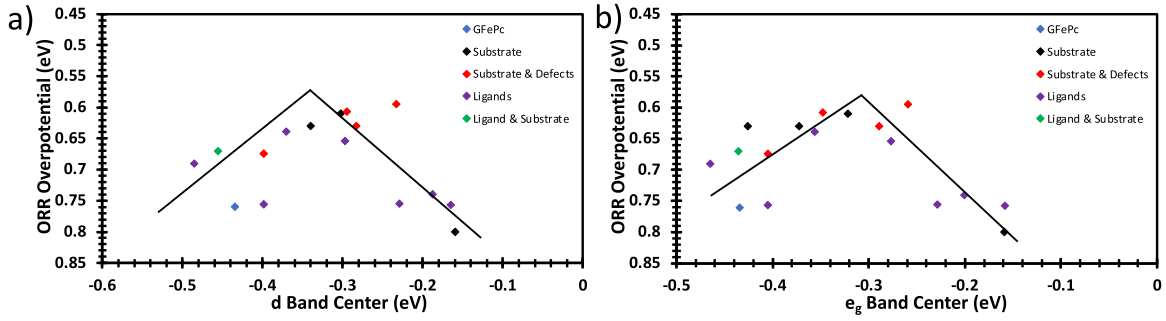

Fig. 15. ORR overpotential plotted against a) *d* and b) e_g bandcenters of Fe.

boron-doping combination into the graphene substrate (MB+SD-GFePc) yielded the lowest ORR overpotential (0.47 eV) and a moderate OER overpotential (0.95 eV) out of the modifications considered when calculated in a water-solvated environment. The enhanced ORR overpotential of the three amino group ligand substitutions tested (16NH_2-GFePc, Para-NH_2-GFePc and Meta-NH_2-GFePc) suggests that ligands with a positive Mesomeric (+*M*) effect and overall electron-releasing group can be favorable toward the ORR overpotential. As most of the ligand and substrate modifications were found to enhance the ORR overpotential to some degree but not the OER overpotential, GFePc and its tested modifications should be mainly studied as a cathode fuel cell catalyst in which the oxygen reduction reaction occurs. Future work should explore a larger range of ligand substitutions that offer varying degrees of Inductive and Mesomeric effects to fully understand the effect the ligand substitution has on the bare catalyst Fe oxidation state and substrate charge. Additionally, other substrate modifications should be explored in conjunction with ligand substitutions to an attempt of reducing the ORR overpotentials of GFePc further.

Credit author statement

N.H. was responsible for performing the simulations, data analysis and writing of the manuscript. P. C. is the senior author responsible for funding acquisition, project administration, and overall supervision.

Declaration of Competing Interest

The authors declare that they have no known competing financial interests or personal relationships that could have appeared to influence the work reported in this paper.

Data availability

Data will be made available on request.

Acknowledgments

Acknowledgment is made to the Donors of the American Chemical Society Petroleum Research Fund for support (or partial support) of this research. The work is supported by ACS-PRF Grant No [58740-UR6]. This work used the Extreme Science and Engineering Discovery Environment (XSEDE) TACC at the stampede2 through allocation [TGDMR140131]. This work utilized resources from the University of Colorado Boulder Research Computing Group, which is supported by the National Science Foundation (awards ACI-1532235 and ACI-1532236),

the University of Colorado Boulder, and Colorado. PCC Cluster, NM Consortium, NM.

Supplementary materials

Supplementary material associated with this article can be found, in the online version, at doi:10.1016/j.mcat.2023.113213.

References

[1] Z. Zhao, Z. Xia, Design principles for dual-element-doped carbon nanomaterials as efficient bifunctional catalysts for oxygen reduction and evolution reactions, ACS Catal. 6 (2016) 1553–1558.
[2] W. Hale, P. Choudhury, Thermodynamic stability and intrinsic activity of La1−xSrxMnO3 (LSM) as an efficient bifunctional OER/ORR electrocatalysts: a theoretical study, Catalysts (2022) 12.
[3] M.K. Debe, Electrocatalyst approaches and challenges for automotive fuel cells, Nature 486 (2012) 43–51.
[4] S. Shen, J. Chen, X. Yan, X. Cheng, L. Zhao, Z. Ren, L. Li, J. Zhang, Insights into properties of non-precious metal catalyst (NPMC)-based catalyst layer for proton exchange membrane fuel cells, J. Power Source. 496 (2021), 229817.
[5] M. Winter, R.J. Brodd, What are batteries, fuel cells, and supercapacitors? Chem. Rev. 104 (2004) 4245–4270.
[6] A. Rabis, P. Rodriguez, T.J. Schmidt, Electrocatalysis for polymer electrolyte fuel cells: recent achievements and future challenges, ACS Catal. 2 (2012) 864–890.
[7] X.X. Wang, M.T. Swihart, G. Wu, Achievements, challenges and perspectives on cathode catalysts in proton exchange membrane fuel cells for transportation, Nat. Catal. 2 (2019) 578–589.
[8] W. Wang, Q. Jia, S. Mukerjee, S. Chen, Recent insights into the oxygen-reduction electrocatalysis of Fe/N/C materials, ACS Catal. 9 (2019) 10126–10141.
[9] Y. Jiao, Y. Zheng, M. Jaroniec, S.Z. Qiao, Design of electrocatalysts for oxygen- and hydrogen-involving energy conversion reactions, Chem. Soc. Rev. 44 (2015) 2060–2086.
[10] C.W.B. Bezerra, L. Zhang, K. Lee, H. Liu, A.L.B. Marques, E.P. Marques, H. Wang, J. Zhang, A review of Fe–N/C and Co–N/C catalysts for the oxygen reduction reaction, Electrochim. Acta 53 (2008) 4937–4951.
[11] E. Proietti, F. Jaouen, M. Lefèvre, N. Larouche, J. Tian, J. Herranz, J.-.P. Dodelet, Iron-based cathode catalyst with enhanced power density in polymer electrolyte membrane fuel cells, Nat. Commun. 2 (2011) 416.
[12] Z. Qin, J. Zhao, 1 T-MoSe2 monolayer supported single Pd atom as a highly-efficient bifunctional catalyst for ORR/OER, J. Colloid Interface. Sci. 605 (2022) 155–162.
[13] X. Li, J. Liu, Q. Cai, Z. Kan, S. Liu, J. Zhao, Engineering d-band center of iron single atom site through boron incorporation to trigger the efficient bifunctional oxygen electrocatalysis, J. Colloid Interface Sci. 628 (2022) 331–342.
[14] D. Wang, L. Jin, M. Liu, T.G. Lee, S.G. Peera, C. Liu, The graphene-supported Lanthanum oxide cluster as efficient bifunctional electrocatalyst for oxygen reaction, Molecul. Catal. 535 (2023), 112879.
[15] L. Jin, C. Liu, D. Wang, M. Liu, T.G. Lee, S.G. Peera, X. Qi, CdN4C0-gra as efficient trifunctional electrocatalyst for the HER, OER and ORR: a density functional theory study, Appl. Surf. Sci. 610 (2023), 155580.
[16] K. Liu, Y. Lei, G. Wang, Correlation between oxygen adsorption energy and electronic structure of transition metal macrocyclic complexes, J. Chem. Phys. 139 (2013), 204306.
[17] F. Jaouen, J. Herranz, M. Lefèvre, J.-.P. Dodelet, U.I. Kramm, I. Herrmann, P. Bogdanoff, J. Maruyama, T. Nagaoka, A. Garsuch, J.R. Dahn, T. Olson, S. Pylypenko, P. Atanassov, E.A. Ustinov, Cross-laboratory experimental study of non-noble-metal electrocatalysts for the oxygen reduction reaction, ACS Appl. Mater. Interface. 1 (2009) 1623–1639.
[18] A. Morozan, S. Campidelli, A. Filoramo, B. Jousselme, S. Palacin, Catalytic activity of cobalt and iron phthalocyanines or porphyrins supported on different carbon nanotubes towards oxygen reduction reaction, Carbon N Y 49 (2011) 4839–4847.
[19] N. Komba, G. Zhang, Q. Wei, X. Yang, J. Prakash, R. Chenitz, F. Rosei, S. Sun, Iron (II) phthalocyanine/N-doped graphene: a highly efficient non-precious metal catalyst for oxygen reduction, Int. J. Hydrogen Energy 44 (2019) 18103–18114.
[20] Y. Jiang, Y. Lu, X. Lv, D. Han, Q. Zhang, L. Niu, W. Chen, Enhanced catalytic performance of Pt-free iron phthalocyanine by graphene support for efficient oxygen reduction reaction, ACS Catal. 3 (2013) 1263–1271.
[21] S. Mussell, P. Choudhury, Density functional theory study of iron phthalocyanine porous layer deposited on graphene substrate: a Pt-free electrocatalyst for hydrogen fuel cells, J. Phys. Chem. C 120 (2016) 5384–5391.
[22] N. Helsel, P. Choudhury, Regulating electronic descriptors for the enhanced ORR activity of FePc-functionalized graphene via substrate doping and/or ligand exchange: a theoretical study, J. Phys. Chem. C 126 (2022) 4458–4471.
[23] G. Kresse, J. Hafner, Ab initio molecular dynamics for liquid metals, Phys. Rev. B 47 (1993) 558–561.
[24] G. Kresse, J. Hafner, Ab initio molecular-dynamics simulation of the liquid-metal–amorphous-semiconductor transition in germanium, Phys. Rev. B 49 (1994) 14251–14269.
[25] G. Kresse, J. Furthmüller, Efficiency of ab-initio total energy calculations for metals and semiconductors using a plane-wave basis set, Comput. Mater. Sci. 6 (1996) 15–50.
[26] G. Kresse, J. Furthmüller, Efficient iterative schemes for ab initio total-energy calculations using a plane-wave basis set, Phys. Rev. B 54 (1996) 11169–11186.
[27] J.P. Perdew, K. Burke, M. Ernzerhof, Generalized gradient approximation made simple, Phys. Rev. Lett. 77 (1996) 3865–3868.
[28] J.P. Perdew, K. Burke, M. Ernzerhof, Generalized gradient approximation made simple [Phys. Rev. Lett. 77, 3865 (1996)], Phys. Rev. Lett. 78 (1997) 1396, 1396.
[29] G. Kresse, D. Joubert, From ultrasoft pseudopotentials to the projector augmented-wave method, Phys. Rev. B 59 (1999) 1758–1775.
[30] P.E. Blöchl, Projector augmented-wave method, Phys. Rev. B 50 (1994) 17953–17979.
[31] S. Grimme, Semiempirical GGA-type density functional constructed with a long-range dispersion correction, J. Comput. Chem. 27 (2006) 1787–1799.
[32] N. Helsel, P. Choudhury, Regulating electronic descriptors for the enhanced ORR activity of FePc-functionalized graphene via substrate doping and/or ligand exchange: a theoretical study, J. Phys. Chem. C (2022).
[33] J.K. Nørskov, J. Rossmeisl, A. Logadottir, L. Lindqvist, J.R. Kitchin, T. Bligaard, H. Jónsson, Origin of the overpotential for oxygen reduction at a fuel-cell cathode, J. Phys. Chem. B 108 (2004) 17886–17892.
[34] P. Choudhury, V.R. Bhethanabotla, E. Stefanakos, Manganese borohydride as a hydrogen-storage candidate: first-principles crystal structure and thermodynamic properties, J. Phys. Chem. C 113 (2009) 13416–13424.
[35] X. Nie, W. Luo, M.J. Janik, A. Asthagiri, Reaction mechanisms of CO2 electrochemical reduction on Cu(111) determined with density functional theory, J. Catal. 312 (2014) 108–122.
[36] A. Ghysels, T. Verstraelen, K. Hemelsoet, M. Waroquier, V. Van Speybroeck, TAMkin: a versatile package for vibrational analysis and chemical kinetics, J. Chem. Inf. Model. 50 (2010) 1736–1750.
[37] G. Dong, M. Huang, L. Guan, Iron phthalocyanine coated on single-walled carbon nanotubes composite for the oxygen reduction reaction in alkaline media, Phys. Chem. Chem. Phys. 14 (2012) 2557–2559.
[38] S. Baranton, C. Coutanceau, C. Roux, F. Hahn, J.M. Léger, Oxygen reduction reaction in acid medium at iron phthalocyanine dispersed on high surface area carbon substrate: tolerance to methanol, stability and kinetics, J. Electroanalyt. Chem. 577 (2005) 223–234.
[39] N. Helsel, P. Choudhury, Enhancing the stability of a Pt-Free ORR catalyst via reaction intermediates, Adv. Mater. Interface. 10 (2023), 2202132.
[40] J. Kotakoski, A.V. Krasheninnikov, U. Kaiser, J.C. Meyer, From point defects in graphene to two-dimensional amorphous carbon, Phys. Rev. Lett. 106 (2011), 105505.
[41] Z. Wang, R. Yin, J. Meng, J. Wang, Y. Liang, C. Ma, S. Tan, Q. Li, J. Yang, B. Wang, Self-limited embedding alternating 585-ringed divacancies and metal atoms into graphene nanoribbons, J. Am. Chem. Soc. (2023).
[42] K. Mathew, V.S.C. Kolluru, S. Mula, S.N. Steinmann, R.G. Hennig, Implicit self-consistent electrolyte model in plane-wave density-functional theory, J. Chem. Phys. 151 (2019), 234101.
[43] K. Mathew, R. Sundararaman, K. Letchworth-Weaver, T.A. Arias, R.G. Hennig, Implicit solvation model for density-functional study of nanocrystal surfaces and reaction pathways, J. Chem. Phys. 140 (2014), 084106.
[44] J.-.L. Fattebert, F. Gygi, Density functional theory for efficient ab initio molecular dynamics simulations in solution, J. Comput. Chem. 23 (2002) 662–666.
[45] R. Jinnouchi, A.B. Anderson, Electronic structure calculations of liquid-solid interfaces: combination of density functional theory and modified Poisson-Boltzmann theory, Phys. Rev. B 77 (2008), 245417.
[46] H.-.F. Wang, Z.-.P. Liu, Formic acid oxidation at Pt/H2O interface from periodic DFT calculations integrated with a continuum solvation model, J. Phys. Chem. C 113 (2009) 17502–17508.
[47] Y.-.F. Li, Z.-.P. Liu, L. Liu, W. Gao, Mechanism and activity of photocatalytic oxygen evolution on titania anatase in aqueous surroundings, J. Am. Chem. Soc. 132 (2010) 13008–13015.
[48] J. Suntivich, J. May Kevin, A. Gasteiger Hubert, B. Goodenough John, Y. Shao-Horn, A perovskite oxide optimized for oxygen evolution catalysis from molecular orbital principles, Science 334 (2011) 1383–1385.
[49] H. Wang, M. Zhou, P. Choudhury, H. Luo, Perovskite oxides as bifunctional oxygen electrocatalysts for oxygen evolution/reduction reactions – a mini review, Appl. Mater. Today 16 (2019) 56–71.